ADVANCED ENGINEERING MATERIALS

DOI: 10.1002/adem.201000259

Five-Parameter Grain Boundary Analysis by 3D EBSD of an Ultra Fine Grained CuZr Alloy Processed by Equal Channel Angular Pressing**

By *A. Khorashadizadeh*, D. Raabe, S. Zaefferer, G. S. Rohrer, A. D. Rollett* and *M. Winning*

The 3D grain boundary character distribution (GBCD) of a sample subjected to equal channel angular pressing (ECAP) after eight passes and successive annealing at 650 °C for about 10 min is analyzed. The experiments are conducted using a dual beam system, which is a combination of a focused ion beam and a scanning electron microscope to collect a series of electron backscatter diffraction (EBSD) maps of the microstructure (3D EBSD). The data set was aligned and reconstructed to a 3D microstructure. The crystallographic character of the grain boundary planes was determined using three different methods, namely, the line segment method, the stereological method, and the triangular surface mesh method. The line segment and triangular surface mesh methods produce consistent data sets, both yielding approximately a 7% area fraction of coherent twins. These results starkly contrast that of the statistical stereological method, which produced a 44% area fraction of coherent twins.

1. Introduction

Grain boundaries play an important role in different processes, such as grain growth and recrystallization, segregation, corrosion, deformation, damage, and oxidation. The structure and properties of the grain boundaries vary in a five-dimensional parameter space as a function of misorientation (three variables) and grain boundary plane orientation (two variables).[1–5] Due to the important role of grain boundaries it is of high interest to characterize and investigate grain boundary character distributions (GBCD) in crystalline materials.

The five-parameter GBCD specifies the fractions of interface area sections, classified according to the three lattice misorientation parameters and the two grain boundary normal parameters.[6,7] Several studies were performed on the five-parameter GBCD of cubic metals[8–12] using stereological approaches that quantify the distribution of grain boundaries in polycrystalline materials on the basis of a set of inter-connected single planar sections. There are also some studies on five-parameter GBCD from direct 3D geometrical data. Saylor *et al.*[13] used a set of calibrated serial sections of

[*] *A. Khorashadizadeh, Prof. D. Raabe, PD Dr. S. Zaefferer, PD Dr. M. Winning*
Department Microstructure Physics and Metal Forming
Max-Planck-Institute für Eisenforschung
Düsseldorf, (Germany)
E-mail: a.khorashadizadeh@mpie.de
Prof. G. S. Rohrer, Prof. A. D. Rollett,
PD Dr. M. Winning
Department Materials Science and Engineering, Carnegie Mellon University, Pittsburgh, (USA)

[**] *One of the authors (MW) expresses her gratitude to the Deutsche Forschungsgemeinschaft (DFG) for financial support through the Heisenberg program. The authors thank the Deutsche Forschungsgemeinschaft for financial support through the project Wi 1917-6/1 within the research unit 544 ''Properties and Interfaces of Ultrafine Grained Materials''. The work at Carnegie Mellon University was supported by the MRSEC program of the National Science Foundation under Award Number DMR-0520425.*

magnesia produced by manual polishing. Rowenhorst *et al.*[14] used the same data acquisition method and analyzed the grain boundary energy of a lead-tin alloy. Dillon *et al.*[15] used the dual-beam system for collecting EBSD maps of Yttria. Li *et al.*[16] have investigated the 3D interfacial network of grain boundaries in polycrystalline nickel using a combination of EBSD mapping and focused ion beam for serial sectioning.

In this study we calculate the five-parameter GBCD of an ultra fine-grained Cu-0.17 wt% Zr sample, produced by equal channel angular pressing (ECAP), from 2D EBSD data and 3D EBSD data sets acquired by an automated dual-beam system.[17–20] The ultra fine-grained CuZr specimen processed by ECAP provides a high density of grain boundaries which is helpful for obtaining good statistics. The 3D EBSD volume probed in this study was about $28 \times 28 \times 17\ \mu m^3$. This volume includes about 91 040 boundary segments, which is a robust quantity for conducting a GBCD analysis.[18] Due to the influence of the grain boundary character on grain growth kinetics, it is the aim of this study to quantify the grain boundaries according to their plane normals and lattice misorientations. The code used for aligning and retrieving the geometry of the grain boundary planes was developed at Carnegie Mellon University by Rohrer and Rollett.[16,20]

In this study we focus on Σ3 grain boundaries, as the misorientation angle distribution of the sample after eight ECAP passes with subsequent annealing at 650 °C for 10 min shows a very large peak in the range 59–62°, Figure 1(a). Figure 1(b) shows the distribution of boundary plane normals independent of the lattice misorientation for the entire data set. It indicates that the population of the grain boundary planes is high at the peak centered on {111} plane. The interface normal analysis shown in Figure 1 was conducted by the triangular surface mesh method which will be explained in detail below.

2. Experimental

The experiments were conducted using a Cu-0.17 wt% Zr alloy. The as-received material was first homogenized for 12 h at 940 °C, then deformed by one ECAP pass, and subsequently annealed at 650 °C for 1 h in order to obtain a homogeneous, fully recrystallized, fine grained structure with an average grain size of 6 μm. Billets with 10 mm × 10 mm cross-section and 60 mm length were then processed by ECAP at room temperature using eight passes via route B_C. This term indicates a 90° rotation about the longitudinal axis of the billet after each pass using the same sense of rotation between the passes. After ECAP deformation, samples of 6 mm × 5 mm × 1 mm (after eight ECAP passes) were cut by spark erosion. The samples were annealed subsequently at 650 °C for 10 min.

The mapping was performed using a dual-beam system for 3D EBSD in a Zeiss XB1560 microscope. The crossbeam instrument is equipped with a field emission electron gun, a Ga^+ ion emitter unit (FIB), and secondary electron, backscatter electron, and scanning transmission electron detectors. For orientation microscopy an EBSD detector (TSL/EDAX software, Hikari S/N 1040 camera) was used. 3D EBSD measurements consist of fully automated serial sectioning and the subsequent high resolution EBSD measurements on each milled layer [18]. The FIB was operated at an accelerating voltage of 30 kV and a 500 pA beam for fine milling. The EBSD measurements were performed at an accelerating voltage of 15 kV. In order to find the precise position after every new cycle a position marker (cross) was milled on the sample surface close to the actual measurement area. This cross was detected at the beginning of each new milling process [18,19]. The spacing between the subsequent slices was 170 nm. The volume analyzed was $28 \times 28 \times 17\ \mu m^3$. The probed volume contained 3093 grains where the threshold for defining a grain was a misorientation angle of at least 5° and 10 voxels minimum grain size. Recent examples of the set-up, the slicing procedure, and the 3D EBSD method are given in [21,22].

3. Data Processing

In this paper we apply three different methods to crystallographically quantify interfaces from 3D and 2D EBSD data sets, namely, the line segment method, the stereological method, and the triangular surface mesh method. The different approaches are schematically illustrated in Figure 2.

The line segment and the triangular surface mesh methods were developed for reconstructing the interfaces in a 3D microstructure with the aim to obtain the GBCD function directly from discrete 3D topological data sets. The stereological method was developed as a statistical measure for calculating the GBCD from observations on a 2D EBSD data set.

In the first approach (line segment method) used for calculating the GBCD, the first step is to reconstruct the grain

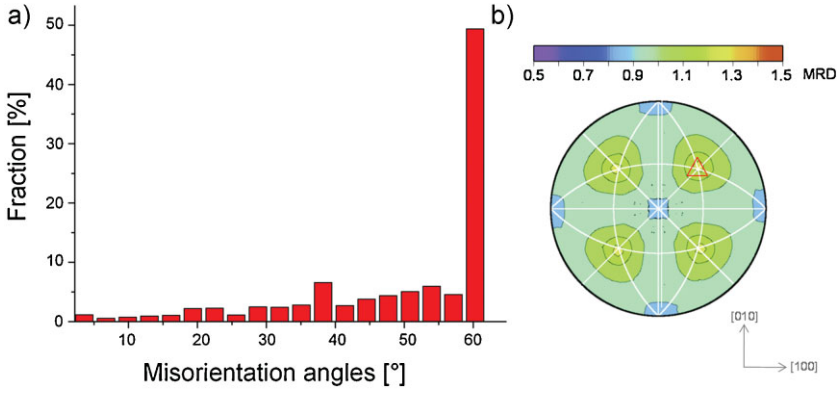

Fig. 1. a) Misorientation angle relative fraction distribution, b) relative areas of the boundary plane distribution, of the sample after 8 ECAP passes with subsequent annealing at 650 °C for 10 min. The red triangle marks the [111] direction (triangular surface mesh method).

ADVANCED ENGINEERING MATERIALS

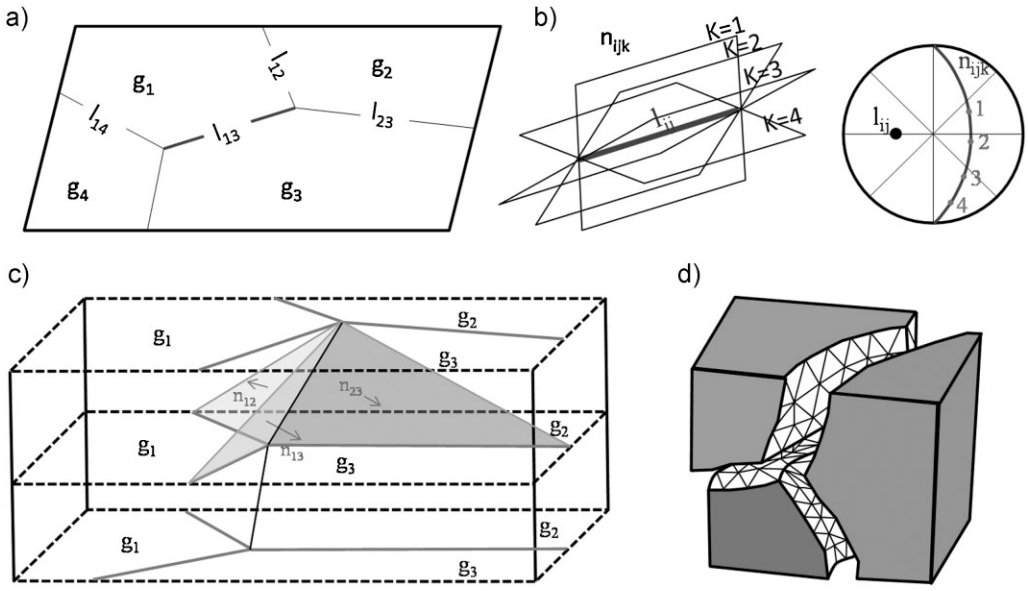

Fig. 2. Schematic representation of a) the statistical stereological method (from 2D EBSD data) and the analysis of interfaces from 3D EBSD data, b) line segment method, and c) triangular surface mesh method. l_{ij} are the grain boundary trace segments in a 2D EBSD data set; n_{ijk} are the unit normals to the possible grain boundaries; k is the possible grain boundary plane; and g_i is crystallographic grain orientation.

boundaries as straight line segments.[15,23] The OIM software was used for reconstructing the straight boundaries from the segment boundaries. The exact approach for building the straight line boundaries used in the OIM software is described in ref.[24] From this step we obtain a list of segments for each layer, which includes information about the average orientation of the grains on either side of the segment in the form of Euler angles (Bunge notation φ_1, ϕ, φ_2), length of the segment, the angle of the reconstructed segments, coordinates of the endpoints in microns, and an integer identifier for the right hand and left hand side grains. The lists including information about the line segments will be used as the input for the software for calculating the GBCD. The method then obtains the triple junctions by identifying all sets of three segments sharing the same coordinate of an end point. These triple junctions in each layer should be matched with the triple junctions on the adjacent layer. The algorithm identifies the five closest triple junctions on the adjacent layer and compares the three crystal orientations on the first layer with the three ones on the adjacent layer. When the disorientation between the crystal orientations is less than 5° a triple line connects the two triple points identified in the adjacent layers. The grain boundary normal will be then determined by the cross product of two vectors of the boundary plane. The discrete grain boundary type of this segment is then determined according to its individual misorientation and boundary normal. Instead of the analysis of the five-parameter GBCD in five-dimensional space, symmetry operations are used to confine the analysis to a sub-domain in which the misorientation parameters vary between 0 and $\pi/2$. This domain, which has a convenient shape for discretization, contains multiple copies of the fundamental zone of misorientations [25] in cubic materials. The plane normal is defined by two angles, namely, the in-plane angle and the azimuthal angle. The azimuthal angle varies between 0 and $\pi/2$ and the in-plane angle between 0 and 2π (for centrosymmetric samples).[17,21]

In the second approach (stereological method), the grain boundary traces (l_{ij}) and the misorientations in a 2D EBSD section of a polycrystalline material are known. Although the normal of the grain boundary plane is not known, it is obvious that it belongs to a set of planes that include the boundary trace in the respective 2D EBSD section and obeys the condition $l_{ij}.n_{ijk} = 0$, where n_{ijk} are a set of C unit normals to the possible grain boundary planes. For each misorientation, sets of n_{ijk} (C cells) are accumulated and weighted according to the length of the observed boundary trace. If there are N observations of traces for a specified misorientation, then there will be N correct boundary normal orientations and N(C-1) incorrect orientations. The technique has been described in detail in ref.[10,17] Although the method can serve as an approximate measure of the interface normal distribution it must be considered that it is retrieved by a statistical method.

In the third approach (triangular surface mesh method), the interfacial areas are discretized into triangular area sets using a generalized marching cube algorithm by which all lines formed by the edges of these triangles will be smoothed.[26] The marching cubes method is a standard iso-surface grid generation algorithm [27] and generates a conformal triangular surface mesh that represents the internal interface structure of the material.

In both, the line segment and the triangular surface mesh methods, it is necessary to properly align the layers before reconstructing and calculating the GBCD. There are two steps

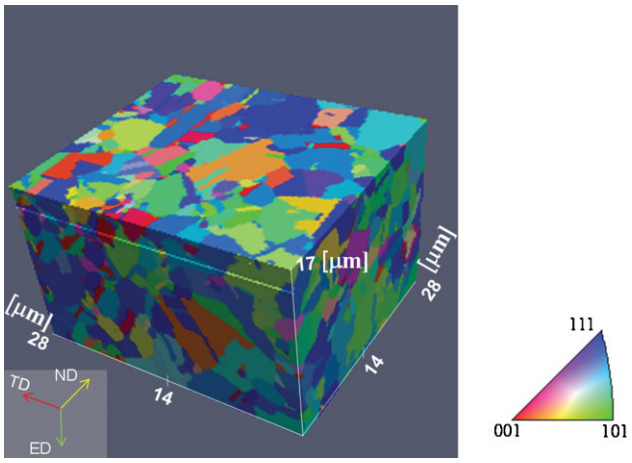

Fig. 3. 3D microstructure of the Cu-0.17 wt% Zr sample after 8 ECAP passes and subsequent annealing at 650 °C for 10 min as obtained from 3D EBSD.[16,17] The color code indicates the crystal directions parallel to ED (extrusion direction). The alignment of the 2D slices is based on minimizing the disorientation between matching voxels in adjacent 2D EBSD layers.[20]

for aligning the layers. The primary alignment code minimizes the disorientation between corresponding voxels between adjacent layers.[20] The secondary alignment performs a rigid shift to the coordinates of the third layer, so that the average triple line direction is perpendicular to the surface.[23]

4. Results and Discussion

Figure 3 shows the 3D microstructure of the sample after eight ECAP passes and subsequent annealing at 650 °C for 10 min. The data set was aligned by minimizing the disorientation between each voxel in adjacent 2D EBSD layers. The microstructure is reconstructed using the ParaView software, an open source visualization software package.[28] The color indicates the crystallographic directions parallel to the extrusion direction (ED) using an inverse pole figure code.

The distribution of the grain boundary planes in the crystal reference frame at the Σ3 interface (60°@[111]) in CuZr after eight ECAP passes and subsequent annealing at 650 °C for 10 min is shown in Figure 2. The symbol Σ defines the volume of the elementary cell of the coincidence site lattice relative to the volume of the elementary cell of the underlying crystal lattice. The coincident site lattice (CSL) concept is a theoretical method for identifying specific misorientations that bring a certain fraction of lattice sites into coincidence when one copy of the lattice is rotated relative to its original position.[29] We used a maximum allowable deviation from the ideal Σ3 boundary of 8.67° according to Brandon's criterion.[30] In this study we compare the results of the discretization of orientation space into 9 bins (corresponding to 10° resolution) and 11 bins (corresponding to 8.18° resolution). The later discretization matches Brandon's criterion reasonably closely.[30]

A pure twist configuration occurs when the grain boundary normal is parallel to the misorientation axis. Σ3 (60°@[111]) boundaries with {111} planes on both sides, are referred to as coherent twin boundaries. The coherent twin boundary inverts the regular A-B-C stacking sequence of close packed {111} FCC layers at the twin boundary plane. Since the nearest and the next-nearest-neighbor atom positions are unchanged, the energy of coherent twin boundaries is very small.[31] Since copper has a low stacking fault energy, the formation of annealing Σ3 boundaries is favorable. Due to this fact, we expect a high fraction of coherent twin boundaries in the material.

Figure 4 represents the GBCD function of the Σ3 interface as calculated from the line segment method. In this figure a relatively strong peak at the Σ3 pure twist boundary position (indicating a coherent twin structure) can be observed. The maximum peak intensity (marked by a red triangle in

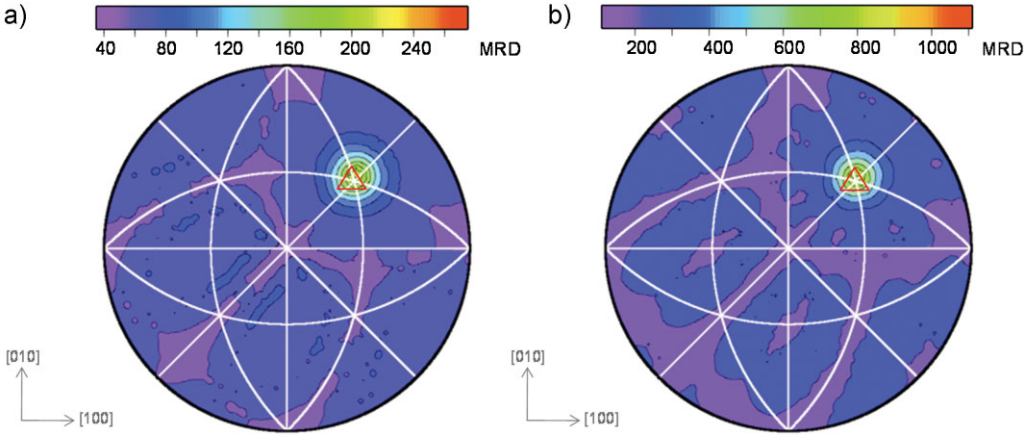

Fig. 4. Grain boundary analysis according to the line segment method obtained from 3D EBSD data for a sample after 8 ECAP passes plus subsequent annealing at 650 °C for 10 min. The results are plotted as a grain boundary plane distribution function for the Σ3 interfaces. a) orientation space is discretized in 9 bins per 90° (coarse angular resolution(10°)), b) orientation space is discretized in 11 bins per 90° (fine angular resolution(8.18°)). The red triangle marks the coherent twin boundaries. Note the different scaling, corresponding to the stronger peak for the higher resolution binning. Both discretization schemes reveal a strong maximum for the coherent Σ3 (60°@[111]) grain boundary (i.e. with a {111} grain boundary plane).

ADVANCED ENGINEERING MATERIALS

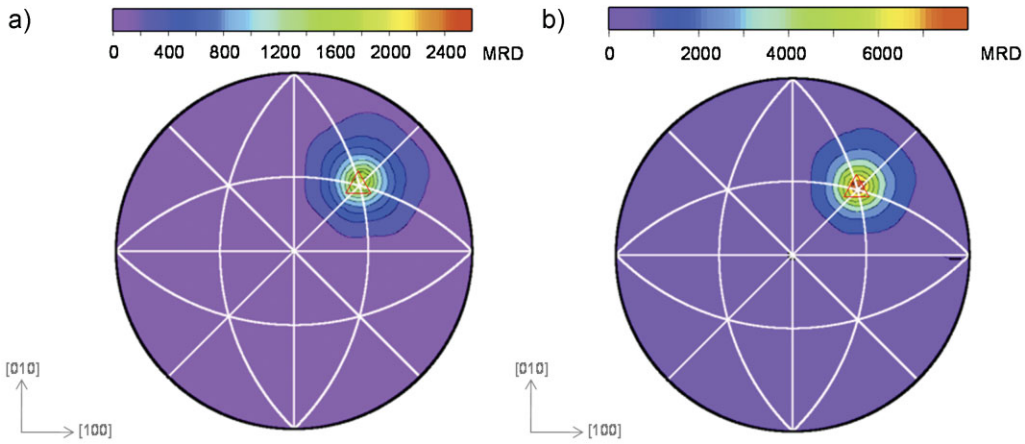

Fig. 5. Grain boundary analysis according to the statistical stereological method from 2D EBSD data plotted for a sample after 8 ECAP passes plus subsequent annealing at 650 °C for 10 min. The results are plotted as a grain boundary plane distribution function for the Σ3 interfaces. a) orientation space is discretized in 9 bins per 90° (coarse angular resolution(10°)), b) orientation space is discretized in 11 bins per 90° (fine angular resolution(8.18°)). The red triangle marks the coherent twin boundaries. Note the different scaling, corresponding to the stronger peak for the higher resolution binning. Both discretization schemes reveal a strong maximum for the coherent Σ3 (60°@[111]) grain boundary (i.e. with a {111} grain boundary plane).

Figure 4) is about 230 multiples of the random distribution (MRD), when the space is discretized in 9 bins per 90°, while the maximum peak intensity for the coherent twin is about 1100 MRD when the space is discretized into 11 bins per 90°. It is apparent that the angular discretization scheme influences the results. Especially in cases such as the Σ3 and higher order coincidence grain boundaries [23] it is, hence, sensible to prefer discretizations that are consistent with the deviations suggested by the Brandon criterion. However, it must also be noted that the finer discretiazation requires more independent observations to populate the bins. We should also consider that the cells in the misorientation sub-domain are parameterized by an angular portion set by φ_1, $\cos(\phi)$, φ_2. The ideal Euler angles of the twin misorientation are $\varphi_1 = 45°$, $\phi = 70.5°$, and $\varphi_2 = 45°$. For the discretization of 9 bins per 90°, the limits of each bin lie at the intervals of 1/9. For the Σ3 twins the $\cos(\phi)$ amounts to 3/9 and falls on the border between the bins. Hence, the intensity of the twin may splits into multiple bins and may appear lower than expected.

Figure 5 shows the GBCD function as calculated from the stereological method. In this approach a 2D EBSD measurement was performed on a large sample section which included about 86000 2D boundary line segments. The result reveals that all Σ3 boundaries are located on the coherent twin boundary planes and the intensity of Σ3 on all other planes is very small. The maximum plane density of the coherent twin boundaries obtained from this stereological approach is about 8 000 MRD for the case where orientation space was discretized into 11 bins per 90° (fine angular resolution of 8.18° according to Brandon's criterion). In contrast, the results obtained from the line segment method (Fig. 4) and the triangular surface mesh method (Fig. 6) show that, although a

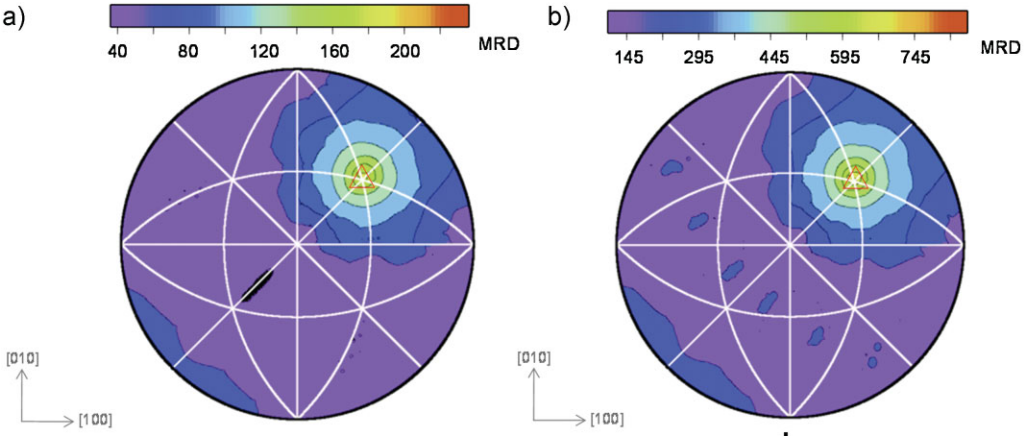

Fig. 6. Grain boundary analysis according to the triangular surface mesh method obtained from 3D EBSD data for a sample after 8 ECAP passes plus subsequent annealing at 650 °C for 10 min. The results are plotted as a grain boundary plane distribution function for the Σ3 interfaces. a) orientation space is discretized in 9 bins per 90° (coarse angular resolution(10°)), b) orientation space is discretized in 11 bins per 90° (fine angular resolution(8.18°)). The red triangle marks the coherent twin boundaries. Note the different scaling, corresponding to the stronger peak for the higher resolution binning. Both discretization schemes reveal a strong maximum for the coherent Σ3 (60°@[111]) grain boundary (i.e. with a {111} grain boundary plane).

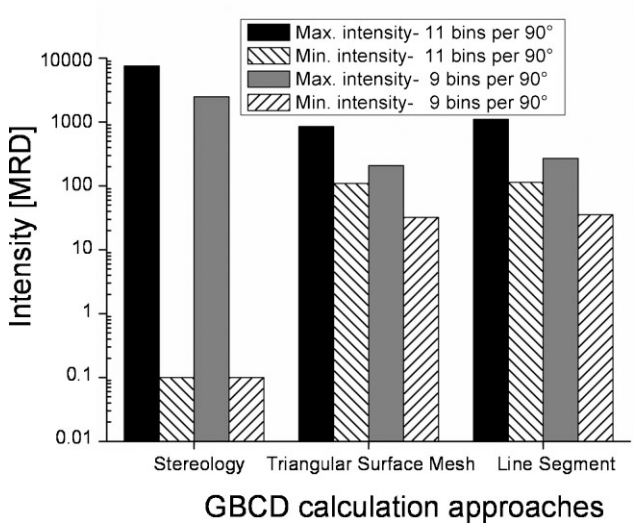

Fig. 7. Maximum and minimum intensity values of the Σ3 GBCD (grain boundary character distribution) functions presented above in MRD (multiples of random) for the three topological approaches: stereology (statistical), triangular surface mesh (discrete), and line segment analysis (discrete). The maximum is at the coherent Σ3 (60°@[111]) grain boundary (i.e. at the {111} grain boundary plane).

strong peak of the Σ3 grain boundary appears at the expected position, not all the Σ3 boundaries are found in an exact coherent twin configuration.

Figure 6 shows the GBCD results obtained from triangulation of the interfacial areas after applying the marching cube algorithm. In this analysis the maximum intensity of the Σ3 boundaries is about 230 multiples of random distribution (MRD) for a discretization of 9 bins per 90°, while the maximum peak intensity for the coherent twin with the discretization of 11 bins per 90° is about 800 MRD. There are slight differences in the maximum and minimum peak intensities between the line segment and the triangular surface mesh methods. However, both 3D analysis methods reveal that not all the Σ3 boundaries are coherent twin boundaries (Fig. 7).

Figure 7 shows the maximum and minimum intensities of the Σ3 grain boundaries in MRD for all three approaches, i.e. stereology, triangular surface mesh, and line segment Analysis. The data reveal three main points. First, the maximum and minimum intensities for Σ3 depend for all three different analysis methods on the angular binning scheme. Second, the triangular surface mesh and the line segment methods which are both obtained directly from generic 3D EBSD topological data sets, provide consistent results. The quite large discrepancy between the stereology approach and the two other methods regarding the ratio of the coherent versus non-coherent Σ3 interfaces is attributed to the influence of preferred textures. The statistical stereological approach might suffer from the fact that once a peak in a real grain orientation distribution occurs (preferred crystallographic texture), other orientations that are close to this maximum in the orientation density may have a more incorrectly assigned length contribution to the interfaces. In the subsequent calculation of the GBCD, the background corresponding to all erroneously accumulated observations is subtracted from the distribution. This will be done under assumption of a random crystal orientation distribution. However, the presence of a preferred ⟨111⟩ texture in the current case leads to an overestimation of the background and, hence, to an incorrect normalization (large subtraction). This lowers the population of incoherent boundaries but has less effect on the intensity of the maximum that is located at the coherent Σ3 interface. The other two analysis approaches are not based on statistics (as the stereological method) but on the direct topological analysis of every single existing boundary in the microstructure. Hence, their analysis results do not suffer from the statistical effects explained above but they are more sensitive to the alignment and possible distortion effects between neighboring 2D EBSD maps that are used for the topological reconstruction.[23] Such misalignments may lead to a broadening effect of the boundary plane orientation distribution away from the peaks and to a drop in the maximum (located at the coherent twin boundaries). Instead the fraction of incoherent Σ3 interfaces is increased. Based on the results from ref.[23], the 3D analysis methods hence typically underestimate the most populous grain boundary plane orientations and overestimate the neighboring plane orientations.

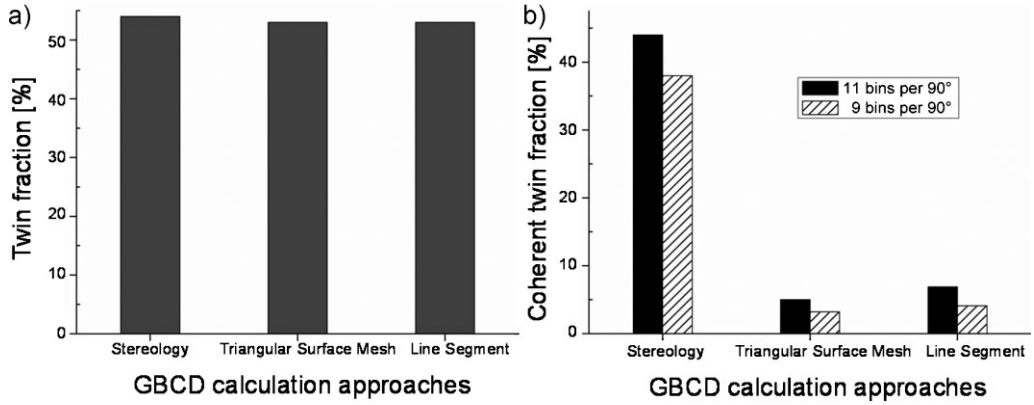

Fig. 8. Area fraction of a) Σ3 twin boundaries b) Σ3 coherent twin boundaries in Cu-0.17 wt% Zr after 8 ECAP passes and subsequent annealing at 650 °C for 10 min from three different approaches: stereological approach; triangular surface mesh method; line segment method.

The intensity of the coherent twin boundaries in the triangular surface mesh approach is slightly lower than the intensity from the line segment method. This may be a consequence of imperfect smoothing performed after triangulation of the interfaces.

Figure 8 underlines these comments as it shows the area fractions of the total Σ3 twin boundary populations and of the coherent Σ3 twin boundaries obtained from the three approaches. Indeed the density of the coherent twins is much larger in the stereological analysis as opposed to the small density found from the two discrete 3D methods [Fig. 8(b)]. When contrasting this result with the density of all Σ3 (60°@[111]) grain boundaries (counting both, coherent and incoherent interfaces) the three methods deliver comparable values [Fig. 8(a)].

Besides the discussion of these differences in the topological robustness of the three algorithms also symmetry aspects must be considered when aiming at extracting meaningful information from grain boundary character distribution functions: If in a cubic system the five angular parameters that characterize a grain boundary are measured at a resolution of 10°, there are approximately 6561 distinguishable grain boundaries. One angular sub domain is $1/64^{th}$ of the entire range. Crystal symmetry effects result in various values of indistinguishable Δg values (misorientations). In a bicrystal there are 2×24^2 equivalent such misorientations. It should also be considered that it is arbitrary whether the grain boundary normal points into the first crystal or into the second crystal. This adds an additional factor of 2 to the symmetrically equivalent boundaries so that we obtain $2 \times 2 \times 24^2(2304)$. This means that there are (2304/64) 36 symmetrically equivalent boundaries in each sub domain. If the sub domain is discretized in 9 bins per 90°, then the number of cells of equal volume will be 4×9^5. Thus for a discretization of 9 bins per 90° the number of distinguishable boundaries is approximately 6 561 ($4 \times 9^5/36$). If the resolution is reduced to 8.18°, we obtain about 17 894 ($4 \times 11^5/36$) distinguishable cells. Due to the equal volume of the cells, the value in each cell is given in terms of MRD. The area fraction of specified grain boundaries can be calculated by dividing the MRD value by the number of distinguishable cells in the sub domain. For example the area fraction of coherent twin boundaries from the stereological approach is about 44% (8 000/17 894) for the discretization of 11 bins per 90°.

5. Conclusions

In this study the grain boundary plane distribution function of Σ3 grain boundaries in a Cu-0.17 wt% Zr alloy processed by ECAP and subsequent annealing was investigated. The crystallographic character of the grain boundary planes was determined using three different methods, namely, the line segment method, the stereological method, and the triangular surface mesh method. The statistical stereological approach showed that practically all Σ3 boundaries are coherent twin boundaries, i.e. they are bounded by {111} planes on either side. The results from two other direct topological (3D) approaches, namely the line segment and the triangular surface mesh method, yielded different results. They revealed that, although the maximum peak of the grain boundary plane distribution function for Σ3 also occurs at the coherent twin boundary position, not all the Σ3 grain boundaries were coherent. Both types of analysis methods contain certain inaccuracies. The 3D analysis is sensitive to the exactness in the alignment between neighboring 2D EBSD layers from which the topological reconstruction proceeds. The effect manifests itself by underestimating the populous boundaries and overestimating the neighbor orientations. In the statistical stereology approach, the occurrence of crystallographic texture effects may artificially lower the population of the incoherent boundaries.

Received: August 27, 2010
Final Version: November 10, 2010
Published online: January 28, 2011

[1] J. E. Turnbull, D. Burke, *Prog. Metal. Phys.* **1952**, *3*, 220.
[2] E. O. Hall, *Proc. Phys. Soc. Lond. Q4* **1951**, Sect. B *64*, 747.
[3] N. J. Petch, *J. Iron Steel Inst.* **1953**, *174*, 25.
[4] T. Tsurekawa, S. Watanabeand, *Mater. Sci. Eng, A* **2004**, *387*, 447.
[5] L. H. Chan, H. Weiland, S. Cheong, G. S. Rohrer, A. D. Rollett, *Ceram. Trans.* **2009**, *201*, 261.
[6] G. S. Rohrer, *JOM* **2007**, *59*, 38.
[7] C. Goux, C. Can, *Metall. Q.* **1974**, *13*, 9.
[8] D. M. Saylor, B. S. El-Dasher, B. L. Adams, G. S. Rohrer, *Metall. Mater. Trans. A* **2004**, *35*, 1981.
[9] V. Randle, G. S. Rohrer, H. M. Miller, M. Coleman, G. T. Owen, *Acta Mater.* **2008**, *56*, 2363.
[10] D. M. Saylor, A. Moraweic, G. S. Rohrer, *Acta Mater.* **2003**, *51*, 3675.
[11] D. M. Saylor, B. S. El Dasher, A. D. Rollett, G. S. Rohrer, *Acta Mater.* **2004**, *52*, 3649.
[12] C.-S. Kim, Y. Hu, G. S. Rohrer, V. Randle, *Scr. Mater.* **2005**, *52*, 633.
[13] D. M. Saylor, A. Morawiec, G. S. Rohrer, *Acta Mater.* **2003**, *51*, 3663.
[14] D. J. Rowenhorst, P. W. Voorhees, *Metall. Mater. Trans. A* **2005**, *36*, 2127.
[15] S. J. Dillon, G. S. Rohrer, *J. Am. Ceram. Soc.* **2009**, *92*, 1580.
[16] J. Li, S. J. Dillon, G. S. Rohrer, *Acta Mater.* **2009**, *57*, 4304.
[17] G. S. Rohrer, V. Randle, *Electron Backscatter diffraction in Materials Science* (Eds: A. J. Schwarz, M. Kumar, B. L. Adams, D. P. Field), Springer, New York **2009**, 215.
[18] S. Zaefferer, S. I. Wright, D. Raabe, *Metall. Mater. Trans. A* **2008**, *39*, 374.

[19] J. Konrad, S. Zaefferer, D. Raabe, *Acta Mater.* **2006**, *54*, 1369.
[20] A. D. Rollett, S. B. Lee, R. Campman, G. S. Rohrer, *Annu. Rev. Mater. Res.* **2007**, *37*, 627.
[21] E. Demir, D. Raabe, N. Zaafarani, S. Zaefferer, *Acta Mater.* **2009**, *57*, 559.
[22] N. Zaafarani, D. Raabe, R. N. Singh, F. Roters, S. Zaefferer, *Acta Mater.* **2006**, *54*, 1863.
[23] G. S. Rohrer, J. Li, S. Lee, A. D. Rollett, M. Groeber, M. D. Uchic, *Mater. Sci. Technol.* **2010**, *26*, 661.
[24] S. I. Wright, R. J. Larsen, *J. Microsc.* **2002**, *205*, 245.
[25] J. W. Zhao, B. L. Adams, *Acta Cryst. A* **1988**, *44*, 326.
[26] S. J. Dillon, S. Lee, A. D. Rollett, G. S. Rohrer, *Microsc. Microanal.* **2008**, *14*, 978.
[27] W. E. Lorensen, H. E. Cline, IEE. Proc. 14th Ann. Conf. Computer Graphics and Interactiv Techniques **1987**, 163.
[28] ParaView: available at: http://www.psc.edu/general/software/packages/paraview/tutorial/.
[29] W. Bollmann, Crystal Defects and Crystalline Interfaces, Springer, Berlin Heidelberg Newyork **1970**, ch. 12.
[30] D. G. Brandon, *Acta Metall.* **1966**, *14*, 1479.
[31] U. Wolf, F. Ernst, T. Muschik, M. W. Finnis, H. F. Fischmeister, *Philos. Mag.* **1992**, *66*, 991.

